

Principal component analysis of minimal excitatory postsynaptic potentials

Andrey V. Astrelin^a, Maxim V. Sokolov^b, Thomas Behnisch^c, Klaus G. Reymann^c,
Leon L. Voronin^{b,*}

^a Department of Mathematics and Mechanics, Moscow State University, Vorobiovy Gory, Moscow, 119899, Russia

^b Brain Research Institute, Russian Academy of Medical Sciences, per. Obukha 5, Moscow, 103064, Russia

^c Department of Neurophysiology, Federal Institute of Neurobiology, Magdeburg, 39008, Germany

Received 6 January 1997; received in revised form 3 September 1997; accepted 16 October 1997

Abstract

'Minimal' excitatory postsynaptic potentials (EPSPs) are often recorded from central neurones, specifically for quantal analysis. However the EPSPs may emerge from activation of several fibres or transmission sites so that formal quantal analysis may give false results. Here we extended application of the principal component analysis (PCA) to minimal EPSPs. We tested a PCA algorithm and a new graphical 'alignment' procedure against both simulated data and hippocampal EPSPs. Minimal EPSPs were recorded before and up to 3.5 h following induction of long-term potentiation (LTP) in CA1 neurones. In 29 out of 45 EPSPs, two ($N = 22$) or three ($N = 7$) components were detected which differed in latencies, rise time (T_{rise}) or both. The detected differences ranged from 0.6 to 7.8 ms for the latency and from 1.6–9 ms for T_{rise} . Different components behaved differently following LTP induction. Cases were found when one component was potentiated immediately after tetanus whereas the other with a delay of 15–60 min. The immediately potentiated component could decline in 1–2 h so that the two components contributed differently into early (< 1 h) LTP1 and later (1–4 h) LTP2 phases. The noise deconvolution techniques was applied to both conventional EPSP amplitudes and scores of separate components. Cases are illustrated when quantal size (v) estimated from the EPSP amplitudes increased whereas v estimated from the component scores was stable during LTP1. Analysis of component scores could show apparent double-fold increases in v which are interpreted as reflections of synchronized quantal releases. In general, the results demonstrate PCA applicability to separate EPSPs into different components and its usefulness for precise analysis of synaptic transmission. © 1998 Elsevier Science B.V. All rights reserved.

Keywords: Principal component analysis; Synaptic transmission; Post-synaptic potential; Quantal analysis; Long-term potentiation; Hippocampus

1. Introduction

Recordings of single-fibre ('unitary') EPSPs or currents are used for studies of synaptic transmission in the central nervous system (CNS), specifically, for quantal analysis (see reviews Redman, 1990; Korn and Faber, 1991; Stevens, 1993; Voronin, 1993; Walmsley, 1993; Thomson and Deuchars, 1995). However, the

unitary EPSPs may consist of several components with different latencies and waveforms because a presynaptic fibre may establish several synaptic connections at various electrotonic distances from the recording site. In practice, instead of unitary EPSPs, so-called 'minimal' EPSPs are often analyzed so that the number of activated fibres can be more than one (Raastad, 1995). Accordingly, the EPSPs may show signs of the presence of different components: notches at the initial slope (Voronin et al., 1992; Alger et al., 1996), bimodal latency distributions (Edwards et al., 1990; Stern et al.,

* Corresponding author. Tel.: +7 095 9179664; fax: +7 095 9160595; e-mail: brainres@dataforce.net

1992; Torii et al., 1997) and different waveforms for different amplitude ranges (Stricker et al., 1996; Voronin et al., 1996). The application of the formal quantal analysis to responses with several components may give false results.

One way to separate different EPSP components is to consider their latencies (Stern et al., 1992; Voronin et al., 1996; Torii et al., 1997). However, the measurements from single trials are not reliable when the latency differences and signal-to-noise ratios are small. A better separation may be achieved using full information contained in both EPSP latencies and waveforms. One way is to use the principal component analysis (PCA). This multivariate technique (Hotellin, 1933; Harmon, 1979; Jackson, 1991) had been applied to CNS studies including the brain imaging (see Friston, 1996 for review), artificial neural nets (Churchland and Sejnowski, 1992) and especially electroencephalographic evoked responses (Glaser and Ruchkin, 1976; Barth and Di, 1992; Chapman and McCrary, 1995). There is an example of PCA of extracellular recordings from retina single cells (Chapman et al., 1981), but to our knowledge there were no attempts to perform PCA on intracellularly recorded EPSPs. Our aims were: (1) to elaborate algorithms suitable for PCA of minimal EPSPs; (2) to test them against lasting intracellular recordings from hippocampal slices; (3) to explore the possibility of analysis of the resulting EPSP components using a variant (Astrelin et al., 1997) of the noise deconvolution which is a standard technique of the quantal analysis (Redman, 1990; Voronin, 1993; Walmesley, 1995).

2. Models and methods

2.1. Principal components analysis

PCA is a mathematical method that finds the most important directions of the data variance in a linear fashion. Detailed discussion of PCA is available in standard texts (e.g. Harmon, 1979; Jackson, 1991). Its electrophysiological applications were reviewed by Glaser and Ruchkin (1976) and Chapman and McCrary (1995). Here we briefly describe a PCA algorithm adapted for analysis of minimal EPSPs with amplitude fluctuations and response failures.

Let $S_i(t)$ be the function describing the waveform of a single EPSP with number i ($i = 1, 2, \dots, N$) from a set of N responses. Let $S_i(t)$ be defined by a set of numbers S_{it} , i.e. we take amplitude measurements from a window of T discrete time points. It is convenient to align the measurements in such a way that the mean amplitude of each single response over the window was equal to 0. The basic assumption of the PCA is that the set of the data waveforms S_{it} can be represented as a linear

combination of K independent fundamental waveforms (components) f_{ik} . In our case, EPSP waveform S_{it} recorded in time bin t on trial i can be represented as a linear combination of responses from K independent inputs plus noise (b_{it}). Therefore

$$S_{it} = \sum_{k=1}^K c_{ik} f_{kt} + b_{it}, \quad (1)$$

where the weighting coefficients or scores c_{ik} indicate the amount of each component present on each trial. Each component (f_{kt}) represents a temporal pattern of component loadings i.e. the morphology of the fundamental waveform of this component (or of k th input in case of EPSP recordings). If we ignore the noise, the following procedure may be used to find the first component (C_1) or f_{1t} . We assume

$$\sum_{t=1}^T f_{1t}^2 = 1 \quad (2)$$

and define C_1 scores as

$$c_{i1} = \sum_{t=1}^T f_{1t} S_{it} \quad (3)$$

Let the 'residual' $S(1)_{it} = (S_{it} - c_{i1} f_{1t})$. From Eqs. (2) and (3) it follows: $\sum_{i=1}^N f_{1t} S(1)_{it} = 0$. Therefore we find f_{1t} so that the sum of respective residuals for all N responses is minimal, i.e.

$$\sum_{i=1}^N \sum_{t=1}^T (S(1)_{it})^2 \rightarrow \min$$

which is equivalent to

$$\sum_{i=1}^N c_{i1}^2 \rightarrow \max. \quad (4)$$

After finding f_{1t} , we calculate the second component (f_{2t}) or C_2 using equations similar to Eqs. (2) and (3), i.e. $\sum_{t=1}^T f_{2t}^2 = 1$, $c_{i2} = \sum_{t=1}^T f_{2t} S(1)_{it}$, the condition of components 'orthogonality' in the space of response amplitudes ($\sum_{t=1}^T f_{1t} f_{2t} = 0$), and a minimization procedure $\sum_{i=1}^N \sum_{t=1}^T (S(2)_{it})^2 \rightarrow \min$. Here the residual $S(2)_{it} = S_{it} - c_{i1} f_{1t} - c_{i2} f_{2t}$. Again similar to Eq. (4), $\sum c_{i2}^2$ is maximized. The procedure can be repeated up to the last component. As a result, each response is described in new coordinates ($c_{i1}, c_{i2}, \dots, c_{iT}$) instead of the previous temporal coordinates S_{it} .

The PCA can be described in terms of signal space geometry (Glaser and Ruchkin, 1976; Harmon, 1979). In these terms, EPSP waveforms are first defined in a data signal vector space of T dimensions so that each data sample represents a single vector. We used $T = 40-80$ so that a window included 0–1.5 ms before the average ($N = 300-2200$) EPSP beginning, initial slope and might include its peak. The task of the PCA was to determine if the same data signal vectors could be adequately represented in a subspace of fewer dimensions. Therefore, the principal components represent

linear combinations of the original EPSP waveforms which explain successively a maximum amount of the system variance and are orthogonal to each other.

In practice, the results of the initial PCA are often difficult to interpret. To obtain a meaningful interpretation of the basic waveforms and their scores, several procedures can be used, most popular being ‘varimax rotation’ (Glaser and Ruchkin, 1976; Harmon, 1979; Jackson, 1991). These procedures produce new ‘components’ that may be useful although they are obtained by different criteria from PCA. Here we elaborated and tested a variant of graphical procedures (Harmon, 1979) suitable for minimal EPSPs (Section 3.1.3).

2.2. Simulation experiments

EPSP waveform (Fig. 1Aa) was described as a function of time by two exponentials: $E(t) = A[\exp(-t/T_{\text{decay}}) - \exp(-t/T_{\text{rise}})]$ where amplitudes A were uniformly or normally distributed. The waveforms were convolved with a Gaussian noise (Fig. 1Ab). The standard deviation (S.D.) of the noise (S_n) was varied in different experiments giving different signal-to-noise ratios. Either non-quantal (continuously distributed) or ‘quantal’ EPSPs were simulated. For the latter, the number of release sites (n) was taken to be one or two. The release probability was usually set at 0.5 so that either about 50% ($n=1$) or 25% ($n=2$) of the waveforms represented failures with zero mean and S.D. equal to S_n . Either ‘small’ ($0.15-0.3v$) or large ($>v$ or $>S_n$) intrinsic quantal variation (S_v) could be added to the non-failures. To simulate two components, different time constants or latencies were introduced, and the two waveforms were mixed so that the sample (typically $N=500$) consisted of failures, mono- and bicomponent waveforms (Fig. 1A).

We tested also influences of response non-linearity. One known example (Martin, 1966) is the nonlinear relation between conductance and potential changes at the postsynaptic membrane which might be expected in dendrites with large local EPSP amplitudes. To imitate the non-linearity, the simulated amplitudes $S(t)$ were transformed into $R(S(t))$ where $R(x)$ is a non-linear function. Either known formulae of non-linear EPSP summation (Martin, 1966) or other asymptotic non-linear functions (e.g. $\arctg(x)$) could be used as $R(x)$.

2.3. Physiological experiments

Hippocampal slices from 5–6 weeks old male Wistar rats were prepared as described previously (Astrelin et al., 1997). The solution in the superfusion experimental chamber contained (in mM): NaCl 124, KCl 1.5, MgCl₂ 1.3, CaCl₂ 2.45, KH₂PO₄ 1.25,

NaHCO₃ 25, glucose 10, picrotoxin 0.1 at 30°C. The recording patch pipettes (2–3 MΩ) was filled with K + gluconate 135, KCl 5, MgCl₂ 2, HEPES 10, glucose 20 (pH 7.2). EPSPs were recorded from CA1 pyramidal cells in the current clamp mode. To avoid the epileptic activity a cut was made between CA3 and CA1 regions and tetrodotoxin (TTX, 2 nM) was added in the perfusion solution. Paired 0.2 ms pulses (50 ms interpulse interval) were delivered to *stratum radiatum* each 6 or 8 s. The stimulus strength (20–50 μA) was adjusted to evoke just suprathreshold (‘minimal’) EPSPs with failures in response to the first pulse in the pair. LTP (Bliss and Collingridge, 1993) was induced by 3 trains (1 s, 100 Hz with 0.4–0.6 ms stimulus duration, 20 s intervals) accompanied by 20 mV depolarization through intracellular current injection. From 120 to 300 responses were collected before tetanization and up to 2000 responses afterwards. After conventional amplification (Patch Clamp L/M-EPC-7, List-Medical, Darmstadt, Germany), data were digitized at 5 kHz and analyzed off line.

2.4. Noise deconvolution

A variant of the noise deconvolution procedure (Redman, 1990) was applied. Peak EPSP amplitudes or component scores were used as input data. Our algorithm (Astrelin et al., 1997) used a L_1 -metric in the space of distribution functions for minimization procedure and applied linear programming methods to decompose the amplitudes (or scores) into a convolution of Gaussian (noise) and discrete distributions. S_v was assumed to be $0.15v$ on the basis of studies on slices from mature animals (Kullmann, 1993; Voronin et al., 1993; Wahl et al., 1995). The pretetanic and post-tetanic recordings were divided into several regions without essential drifts. Each region contained from 100 to 400 trials. The weighted mean interval between the components of the deconvolution solution (i.e. resulting discrete distribution): was used to define $v = x_i * P_i / \sum i * P_i$. Here x_i , location (distance from 0) of component i and P_i , its probability. The mean quantal content (m) was evaluated as the mean amplitude (or component score) divided by v . ‘Significant differences’ correspond to $P < 0.01$ (t -test).

3. Results

3.1. Simulation experiments

The aims of the simulation experiments was to test PCA algorithms, to assist elaboration of the alignment procedure (Section 3.1.3) and to facilitate interpretation of the physiological results.

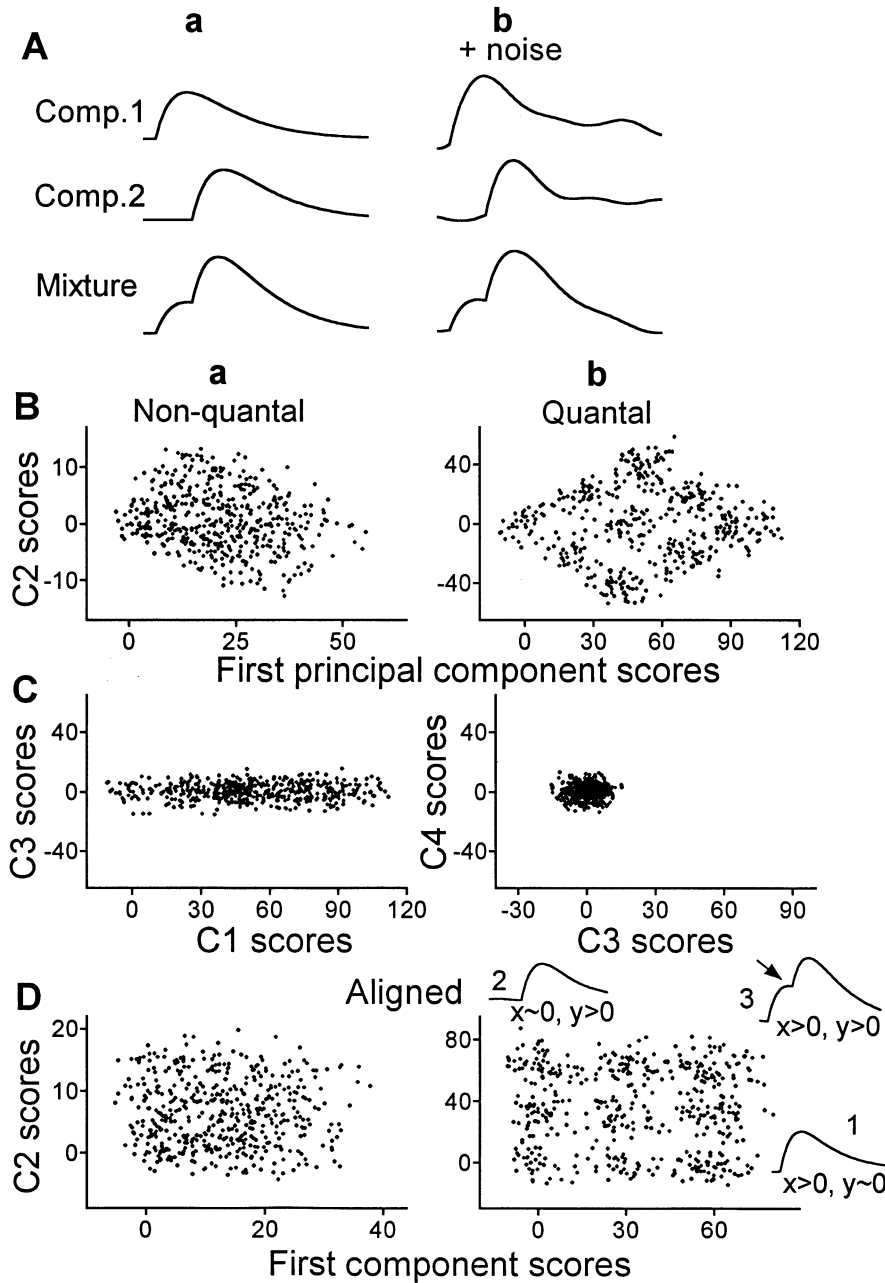


Fig. 1. Principal component analysis of simulated waveforms. Two waveforms with different latencies and with response failures were simulated and mixed. Either non-quantal or quantal release with two release sites was suggested. (A) Simulated waveforms with shorter (Comp. 1) and longer (Comp. 2) latencies and also their mixture (column a) and the same waveforms contaminated with noise (column b). (B) Plot of the scores of the two initial principal components from the experiments with simulations of non-quantal (a) and quantal (b) waveforms. Note characteristic parallelograms suggesting the presence of two components. (C) The scores of the third principal component plotted against the first (a) and the fourth (b) ones. Note the narrow band (a) and the cloud (b) suggesting that the third and fourth components were absent. (D) ‘Alignment’ procedure and extraction of the simulated waveforms. The plots a and b represent transformed (‘aligned’) plots of Ba and Bb, respectively. Note that the parallelograms of B transformed into rectangular fields. Insets (1–3) show waveforms obtained by averaging the simulations corresponding to the dots from different parts of the plots in b: 1, for the band along the x -axes with y values within $0 \pm 2S_{y,}$; 2, for the band along the y -axes with x values within $0 \pm 2S_{x,}$; 3, for the cloud with both x and $y > 2S_{x,y}$. Note that the procedure restores the waveforms (Db, 1–3) identical to the simulated ones (A). The arrow (Db3) marks the notch corresponding to the beginning of the longer-latency component. 500 waveforms were simulated in each of the experiments shown here and in Figs. 2–6.

3.1.1. ‘Optimization’ of the number of PCA components

The importance of PCA is its ability to adequately represent a T variable data set in $K < T$ dimensions.

The larger K , the better fit of the PCA model; the smaller K is, the more simple model will be. Determination of the optimal value of K (‘when to stop?’, see Jackson, 1991) is essential: it permits to ignore compo-

nents that explain very little of the total variance and, in addition, may not be readily interpretable. There are a large number of the respective criteria (Jackson, 1991) but generally the problem of K determination does not seem to be solved.

In our case, the components which describe noise do not represent any essential interest. Therefore, to optimize K we compared PCA results obtained from the responses and from the background noise. The idea was formulated as follows. Let define for every k from Eq. (1) $w_k = (1/N) * \sum_{i=1}^N (c_{ik})^2$ which is the squared mean deviation of the PCA scores from 0. Let represent the background noise as values B_{it} in the same way as S_{it} (Section 2.1). Now let obtain its scores h_{ik} in the same PCA basis: $h_{ik} = \sum_{t=1}^T B_{it} f_{kt}$ and calculate $d_k = (1/N) * \sum_{i=1}^N (h_{ik})^2$. If a component does not contain any information about the response i.e. it corresponds to the noise, w_k should be approximately equal to d_k where $k = 1, 2, \dots, T$ is the number of the components. Therefore we considered the sequence $o_k = w_k/d_k$ which was decreasing and tended to approach 1. According to our criteria we can ignore components which give o_k smaller than a certain constant (e.g. 1.2). We shall see below that the two-dimensional (2D) plots of the last simulated component against the next (non-simulated) component represented a band (Fig. 1Ca) with the width comparable to that of the respective plot for the noise, i.e. passing the above criterion. In practice, on the basis of the analysis of physiological data (see below) we used $K = 5$.

3.1.2. Basic PCA analysis

Fig. 1 considers the algorithm implementation using simulated EPSPs (Fig. 1A) with two components having different latencies. The first step was to input the chosen parts (Section 2.1) of the simulated waveforms for calculation of the PCA scores. The second step was to consider the 2D plot of the scores of the two initial principal components. The illustrated plot (Fig. 1Ba) represented a parallelogram with an apex at (0, 0) which was typical for bicomponent simulations. The next step was to consider similar plots between C_1 or C_2 and later (C_3 – C_5) components. The C_1/C_3 plot (Fig. 1Ca) represented a band with the width comparable to that of the noise indicating the absence of C_3 (see Section 3.1.1). The C_3/C_4 plot (Fig. 1Cb) was practically indistinguishable from the noise plot. Bands similar to Fig. 1Ca were observed for other combinations of C_1 or C_2 with later components and the noise clouds similar to Fig. 1Cb were observed for other components which had not been simulated. Summarizing, the above considerations are in agreement with the simulation of the two-component EPSP.

The band-like plots similar to Fig. 1Ca were observed also when only one component was simulated (Fig. 2Aa). For simulations of the waveforms with

variable kinetics (Fig. 2Ba) the dots outlined a ‘fan’ starting from (0, 0) coordinate. Non-linear cases (Fig. 2Ca) created curved plots. In the two latter cases (Fig. 2Ba, Ca), the width depended on S_n as well as on the waveform variability or the degree of the non-linearity, respectively. For comparison, Fig. 2D illustrates a simulation of two components with the same latency but different kinetics. It represented a parallelogram typical for the bicomponent plots (Fig. 1Ba).

The ‘quantization’ did not change general shapes of the plots in the linear cases (Fig. 1Bb, Fig. 2Ab and Db), except separation of the cloud of failures around the coordinate (0, 0) and additional groupings of component scores. Fig. 1Bb illustrates simulations with two quantal levels and small S_v (see Section 2.2); Fig. 2Ab–Db represent monoquantal responses with $S_v > S_n$.

3.1.3. Alignment procedure and component identification

If K is the ‘optimal’ number of components (Section 3.1.1), we can consider the following signal representation instead of Eq. (1): $S_{it} = \sum_{k=1}^K c_{ik} f_{kt} + R_{it}$, where R_{it} is a small residual which we can ignore. To facilitate physiological interpretation (Section 2.1) we can define new functions F_{it} so that $S_{it} = \sum_{i=1}^K C_{il} F_{it}$. We shall look for F_{it} in the form: $F_{it} = \sum_{k=1}^K A_{ik} f_{kt}$. Therefore, $f_{kt} = \sum_{i=1}^K A'_{ki} F_{it}$ where the matrix A' is the inverted matrix A . Then $C_{il} = \sum_{k=1}^K c_{ik} A'_{ki}$ i.e. the coefficients C_{il} can be obtained from c_{ik} in Eq. (1) by a linear transformation. To facilitate component identification we performed a transformation of the 2D plots according to the following: (1) The dots around (0,0) coordinate should preserve their position within $\pm 2S_n$ (where S_n is the noise S.D. for respective component). This condition follows from the above formulations of the linear transformation of the coefficients c_{ik} into C_{il} . (2) All C_{il} should be positive within $\pm 2S_n$. This condition is natural for purely excitatory inputs. (3) The borders of the component plots (Fig. 1Ba,b) should be aligned along the coordinate axes (Fig. 1Da,b). The objective was to obtain a full range of ‘pure’ component scores for one input (response component) which corresponds to about zero values for the other input. This condition stresses one limitation of our identification procedure: the presence of response failures for every component to be unequivocally identified. (4) If the plot contains gaps (Fig. 1Bb and Fig. 2Db) they should also be aligned. This condition is natural because the gaps reflect ‘quantization’ which creates additional borders. They facilitated the alignment (see below) especially when N and the number of failures (N_0) were low.

Therefore, the further step of our analysis was the alignment of the visually inspected C_1/C_2 plots (Fig. 1Ba). We used a computer algorithm based on the above conditions. The result of the alignment of Fig.

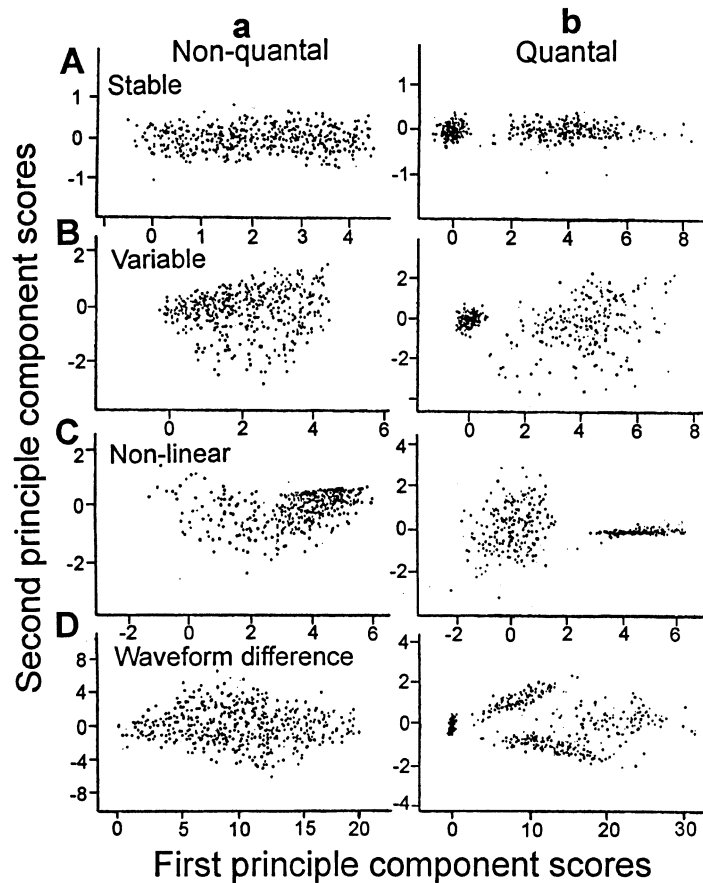


Fig. 2. Comparison of the PCA of simulated waveforms with one (A–C) and two (D) components. The scores of the two initial principal components are plotted. Columns a and b represent simulations of non-quantal and monoquantal waveforms, respectively. The simulated monocomponent EPSPs (A–C) has a stable waveform (A), waveform variations (B) or non-linear measurements (C) based on $\arctg(x)$ transform (Section 2.2) of a stable waveform. (D) Simulations of EPSPs with two components having different response kinetics but the same latency. Note the band-like shape of the plot in the monocomponent cases (A), the fan-like plot in B, complicated fields in C and the parallelograms in the bicomponent cases (D).

1Ba is shown in Fig. 1Da. It gave a rectangular plot typical for bicomponent cases. As noted, the quantization (Fig. 1Bb) facilitated the alignment (Fig. 1Db) due to gaps and additional borders.

The aligned plots were used to interpret the meaning of the components and to ‘restore’ the simulated waveforms. We averaged the waveforms which corresponded to about 0 scores (within $\pm 2S_n$) for all coordinates except one (Fig. 1Db, insets 1 and 2). For example, Fig. 1Db1 was obtained by averaging the waveforms corresponding to the dots along the x -axes with y values close to 0. Fig. 1Db2 represents the dots along the y -axes. The recovered components (Fig. 1Db1, 2) were identical to the simulated waveforms with different latencies (Fig. 1Aa). Accordingly, the averaging of the simulations corresponding to both x and y positive (Fig. 1Db3) was identical to the mixture of the simulated components (Fig. 1Aa). The inflection point (Fig. 1Bb3, arrow) corresponded to the beginning of the longer latency component.

Fig. 3A illustrates aligned plots for simulations of two components having the same latency but different kinetics (Fig. 2D). Insets 1–3 (Fig. 3A) give the results of the recovery of the simulated components with the fast (Fig. 3A1) and slow (Fig. 3A2) kinetics as well as their mixture (Fig. 3A3) using the above averaging procedure. The result was in complete agreement with the actually simulated waveforms.

In contrast to the bicomponent cases (Fig. 1D and Fig. 3A), the alignment of the variable waveforms (Fig. 2B) gave the plot (Fig. 3B) with a negative correlation and with the shape close to a triangle rather than to a square. The star in Fig. 3Ba denotes the blank region without cases with large C_1 and C_2 scores. This agrees with the fact that no independent components were simulated. The plots with waveform variations (Fig. 2B) were more difficult to align, especially with small N (< 200) and large noises ($v/S_n < 2$) due to less clear borders as compared to the bicomponent plots (Fig. 1B and Fig. 2D). For the variable waveforms (Fig. 3B), the above averaging procedure resulted in appearance of

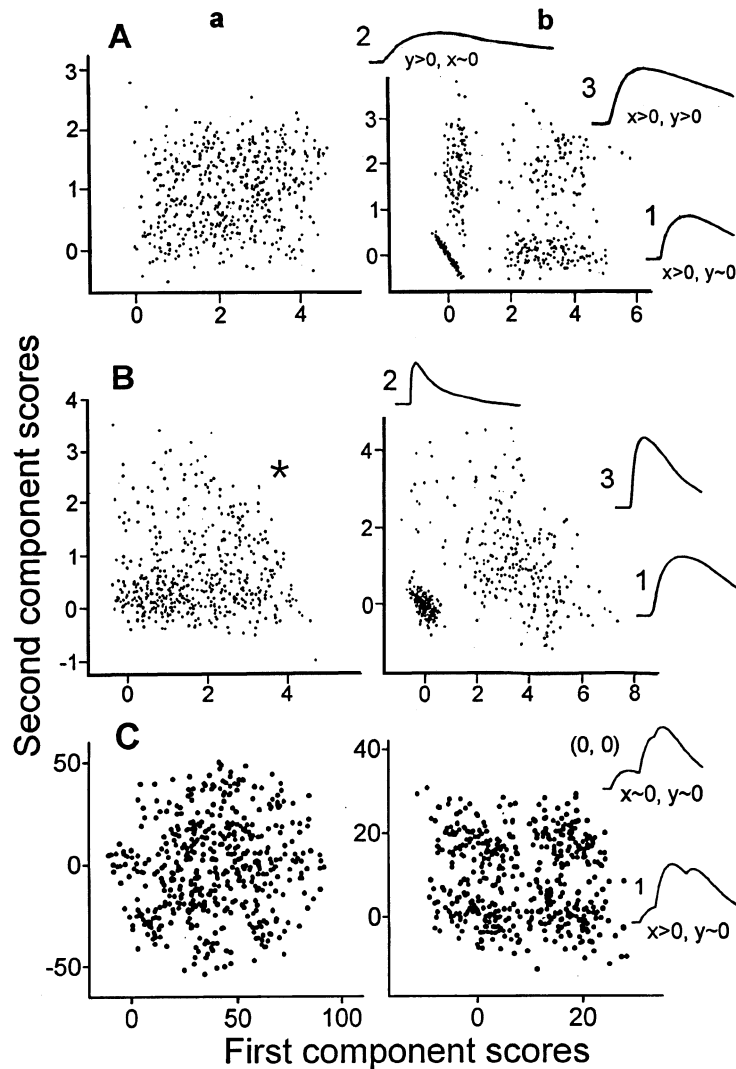


Fig. 3. 'Alignment' of the PCA scores and extraction of the simulated waveforms in experiments with simulations of two (A, B) or four (C) components. The components had different kinetics (A), waveform variations (B) or different latencies (C). (A, B) Transformed ('aligned') plots of Fig. 2D and 2B, respectively, with simulations of non-quantal (a) and monoquantal (b) EPSPs. Note that the parallelograms of Fig. 2D representing bicomponent waveforms transformed into a square (A) whereas the 'fan'-like plot for the variable waveform (Fig. 2B) transformed into a triangle (B). The star indicates the lack of waveforms having large scores for both components. Insets 1–3 in Ab show waveforms obtained by averaging the EPSP simulations corresponding to different parts of the plots (see Fig. 1D legend for more details). The averages 1 and 2 were identical to the simulated components with different kinetics; the inset 3 represents the mixture of 1 and 2. Similar averages in B (1–3) reflect variations of the simulated waveform. (C) Initial (a) and aligned (b) plots from an experiment with simulations of four monoquantal components with different latencies (5, 15, 25 and 35 conventional units) and fixed rise time (10 units). Insets (0, 0) and 1 show waveforms obtained by averaging the simulations corresponding to the failure cloud and to the positive x values with about 0 y values, respectively. They contain two and three additional longer latency components, respectively.

waveforms with different kinetics (Fig. 3B1–3). The result was also in agreement with the simulations used for Fig. 3B because the simulated rise and decay times varied between those obtained in Fig. 3B1 and B3. However, by itself the result did not decide whether the initial data (Fig. 2Bb) contained discrete components or represented a continuum of variable waveforms. Our simulations showed that to answer this question one should first analyze the C_1/C_2 plots (Fig. 2) and to try to align them (Fig. 3). The rectangular plots without correlations (Fig. 1D and Fig. 3A) would indicate

occurrence of two independent components whereas a triangle structure with a blank sector (Fig. 3Ba, star) would suggest waveform variations.

3.1.4. Simulations of more than two components

The simulations of the variable waveform (Fig. 3B) imitate also cases with a large number of different components, each appearing with a low probability. When three or four independent components were simulated, the initial C_1/C_2 plots (Fig. 3Ca) had a more complicated shape as compared to the parallelograms

of the bicomponent plots (Fig. 1B). It represented a hexagon- or an octagon-like field for three or four simulated components, respectively. The absence of clear borders made the alignment difficult. It was possible to perform only at high signal-to-noise ratios ($v/S_n > 2.5$) with clear quantal groupings (Fig. 3Cb). At lower v/S_n or non-quantal simulations, considerations of the plots of different PCA components could indicate the presence of > 2 simulated components, but their separation was not possible. In the illustrated case with large latency differences between four simulated components (Fig. 3C), 16 clouds in 4D space were observed. After their alignment, every 2D plot ($(C_1/C_2, \dots, C_2/C_4)$) contained four clouds as in the illustrated C_1/C_2 plot (Fig. 3Cb). Insets in Fig. 3Cb show that the averaging procedure applied to the 2D plots confirmed existence of several components but did not separate them. One characteristic difference from the bicomponent simulations is the presence of the responses at the average corresponding to about (0, 0) coordinates (Fig. 3Cb). Our algorithm included an option for the averaging in a multidimensional space. In addition to the high v/S_n , a sufficiently high N_0 for each component was necessary for the complete component separation using this algorithm.

3.1.5. Exploration of different signal-to-noise ratios

Limits of the resolution of the identification procedures were explored in over 60 simulations of variable signal-to-noise ratios (Fig. 4), T_{rise} and latencies (Fig. 5). In the experiment of Fig. 4 (column b) we simulated one biquantal and one monoquantal component with different latencies. We diminished v for the latter from A to E so that v/S_n decreased. The width of the failure cloud (at the (0, 0) coordinate) in Fig. 4Ab and Bb was comparable to that of the noise cloud (Fig. 4Aa) because S_n was constant. However the width of the gap between the upper and lower rows diminished when v/S_n decreased. Nevertheless, even at $v/S_n = 2$ (Fig. 4Cb) it was possible to apply the averaging procedure (Section 3.1.4) to identify C_1 (Fig. 4C1) and C_2 (Fig. 4C2). At smaller v/S_n (Fig. 4Db and Eb) the rectangular plot (Fig. 4Ab–Cb) regressed to a band with the width comparable to that of the noise cloud (Fig. 4Aa) so that the plot became similar to those for monocomponent cases (Fig. 2A, Section 3.1.1). Nevertheless, it was possible to extract C_2 (Fig. 4Eb2) using responses corresponding to the failure cloud. Therefore, the present algorithm provides a method to identify a component with the amplitude well below the noise level provided that another component has a sufficiently large N_0 and signal-to-noise ratio. Note, however, that the scores of the noisy component are not suitable for quantal analysis (see below).

Column c (Fig. 4) shows variations of v/S_n for both biquantal components. The groupings and gaps (Fig.

4Ac) became less prominent with decreased v/S_n (Fig. 4Bc) and disappeared at $v/S_n < 2$ (Fig. 4Dc) so that the plot became similar to those for non-quantal cases (Fig. 1Da, Fig. 3Aa). At even smaller v/S_n (Fig. 4Ec), the plot lost clear borders so that both alignment and component separation became problematic.

3.1.6. Exploration of different latencies and rise times

In Fig. 1, the component latencies differed for four times. Fig. 5A and B presents C_1/C_2 plots before (a) and after (b) alignment for the same waveforms and with the same $v/S_n = 2.5$ but with decreasing differences (ΔL) between the latencies of the first and the second components (L_1 and L_2). In Fig. 5Aa and Ba the quantal groupings and gaps were visible and the plots had clear borders. The alignment was easy to perform and resulted in the characteristic rectangles (Fig. 5Ab and Bb). However, at less than two-fold latency difference the initial plot (Fig. 5Ca) became close to the band-like monocomponent plots (Fig. 2A). The alignment (Fig. 5Cb) did not produce a rectangle with clear borders so that component separation became generally unreliable. Nevertheless, averages corresponding to different parts of the plot (Fig. 5Cb1–3) had different latencies indicating the presence of different components. Our simulations showed that when the components had different latencies, a criterion for the presence of two components is the absence of intermediate latencies in the parts of the plot presumably corresponding to the component mixture (Fig. 5Cb3). Otherwise, the plot corresponds to latency variations either due to the intrinsic properties of the response or to noise contamination. It is clear that analogous criterion was impossible to use for waveforms with different T_{rise} having the same latencies because the component mixture should have intermediate T_{rise} independent of whether separate components exist or not. It should be stressed that when the plot has no clear borders and the alignment does not produce a rectangular, the components can be detected (*identified*) but not completely *separated* so that the scores of the individual components can not be used for further analysis.

Fig. 5Da illustrates simulations with even smaller than in Fig. 5Ca latency differences but with two monoquantal components having 50% difference in v . The additional difference improved the groupings and gave a possibility to resolve the components (Fig. 5D, insets 1 and 2).

Our simulations showed that the ratio $\Delta L/T_{\text{rise}}$ is more important variable as compared to ΔL by itself. Fig. 5 (column c) illustrates experiments with variable T_{rise} in two components having fixed latencies. Fig. 5Dc shows that at too small $\Delta L/T_{\text{rise}}$ the plot lost parallelogram shape with clear borders (Fig. 5Ac–Cc) so that its alignment and component separation became impossible.

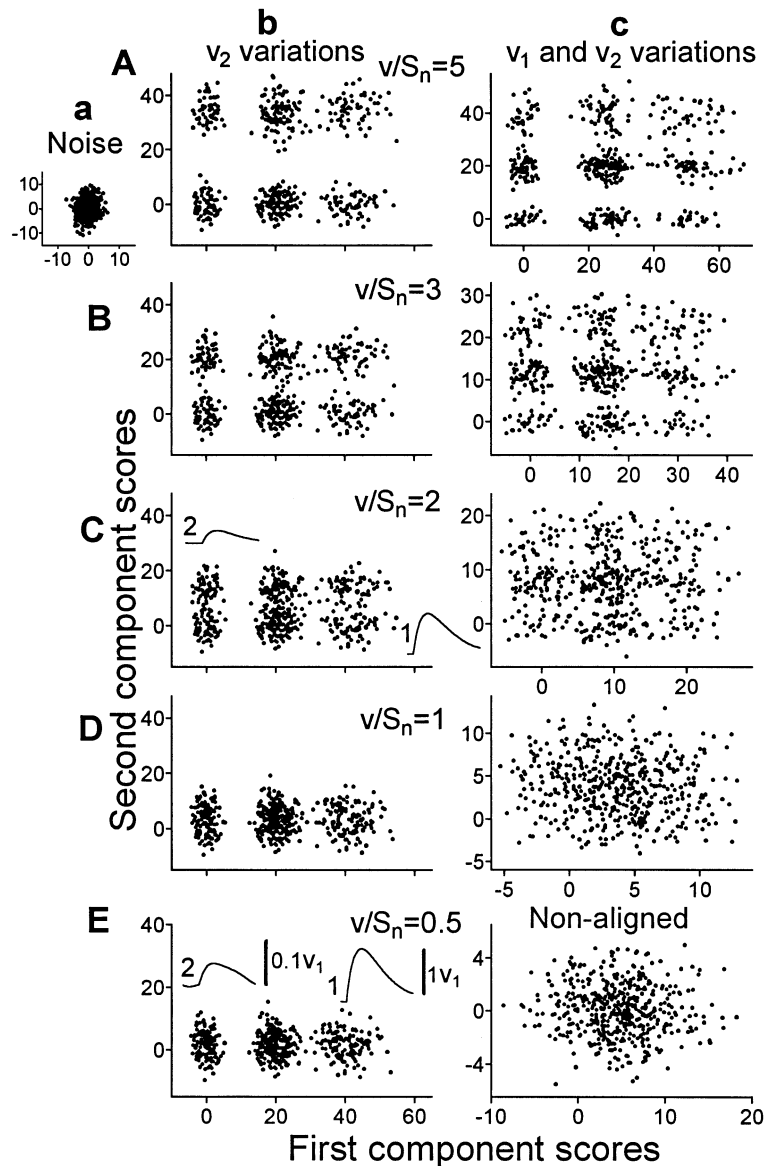


Fig. 4. Simulation experiments aimed to study the PCA algorithm resolution at varying signal-to-noise levels (A–E). Aa and columns b and c represent C_1/C_2 plots for the background noise and for two experiments with simulations of bicomponent EPSPs, respectively. The first component was biquantal with a shorter latency and the second one was monoquantal for b and biquantal for c with four-times longer latency. Binomials with $p = 0.5$ and $n = 1$ or 2 were used to imitate the quantal release. For b the quantal size (v) was fixed at $v/S_n = 5$ for the first component, and it was decreased for the second component from A to E to create various v/S_n ratios as shown. The actual signal-to-noise ratio decreased from 2.5 to 0.25 because 50% of C_2 simulations represented failures. Note that at $v/S_n \geq 2$ (A–C, b) the two components can be clearly resolved. 1 and 2 in C represent averages obtained with the selection procedure (see Fig. 1D legend). The width of the plots at $v/S_n \leq 1$ (D, E, b) was comparable to that of the noise (Aa). Nevertheless, averaging of the failures of the first component (Fig. 4E2) reveals the second component with amplitude < 0.05 as compared to the first component (Fig. 4E1). For column c, amplitudes of both components was diminished relative to S_n by decreasing v . At $v/S_n < 1$ (Ec) the plot represents a cloud which can not be aligned because of the lack of distinct borders.

Fig. 6A–C summarizes additional simulations with variations of v/S_n , latencies and T_{rise} . The ordinates present the normalized C_2 width in initial (non-aligned) C_1/C_2 plots. The dashed line marks the C_2 width (1.2) at which the component resolution became generally unreliable. Comparisons of circles and squares in Fig. 6A and also of Fig. 6B and C show that the analysis is more sensitive to latency as compared to T_{rise} differences. Thus, at equal latencies (Fig. 6C, circles) only

components with several-fold T_{rise} differences could be resolved at $v/S_n = 2$. At equal T_{rise} (Fig. 6B), small relative latency differences could be resolved even at smaller v/S_n . It should be stressed that Fig. 6A–C represents simulations of monoquantal responses and therefore evaluates the lower limits of the algorithm resolution. Note also that the algorithm became essentially more sensitive when both latency and T_{rise} were different (Fig. 6A and C, dots).

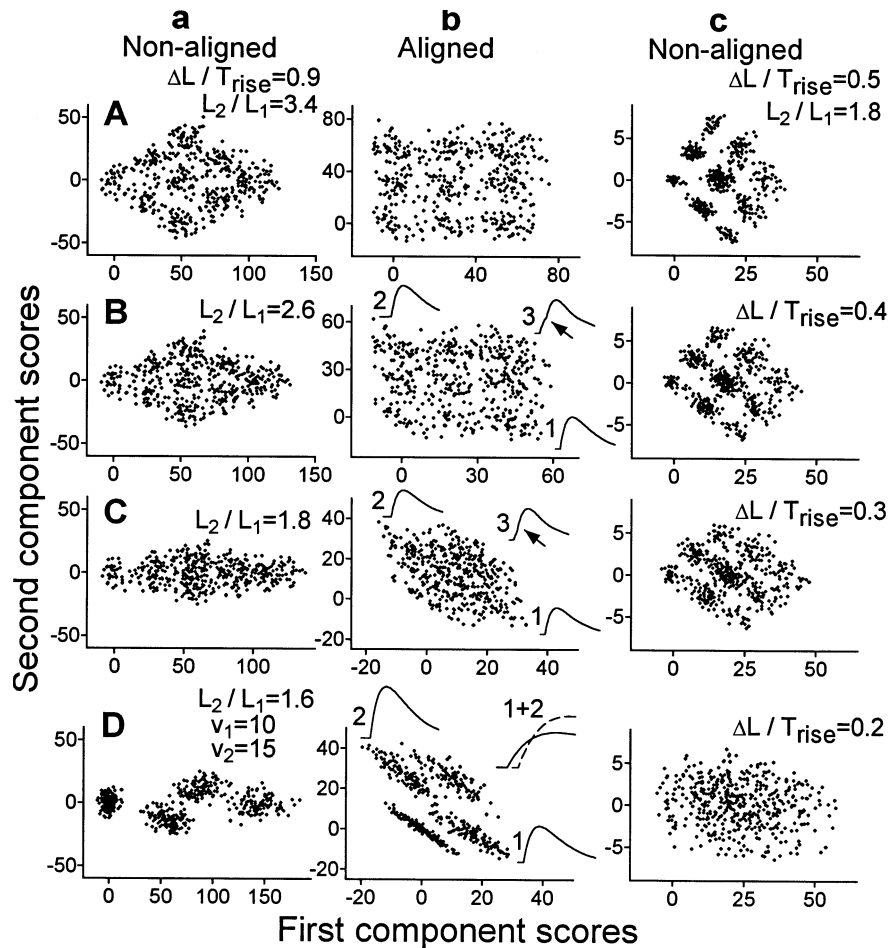


Fig. 5. Simulation experiments to study the PCA resolution with variations of latency differences (ΔL in a, b) and ratios between the latency difference and rise times ($\Delta L/T_{\text{rise}}$ in c). In a and b, the latency of the second component (L_2) was diminished from A to C so that the latency ratios (L_2/L_1) were varied as indicated. Averages 1–3 were obtained as in Fig. 1D. At $L_2/L_1 < 2$ (Ca) the plot became close to a band and the alignment became difficult because of the lack of clear borders (Cb). Nevertheless, the averages from different parts of the plot gave waveforms with different latencies (Cb1 and 2). The short latency of the average from the intermediate area (Cb3) indicates the presence of two components rather than a continuum of latency variations. Da and b represent a simulation of two monoquantal components with different v . Note that separation of the components became easier in spite of even smaller latency differences than in Ca and b. D1 and D2 show averages corresponding to the adjacent clouds. Db, 1 + 2 represents their superposition at an expanded time scale to demonstrate the latency difference. Column c represents simulations of bicomponent EPSPs with different T_{rise} but fixed latencies (5 and 9 conventional units). Note that the plot lost clear borders and became not suitable for alignment when the latency difference became too small as compared to T_{rise} (Dc). Because T_{rise} was varied in column c, the width of the window for EPSP measurements was increased from A to D.

3.2. Physiological experiments

3.2.1. Examples of EPSPs and their potentiation

Fig. 7A and Fig. 8A exemplify our recordings. Comparisons of the first (EPSP1) and second (EPSP2) responses show typical paired-pulse facilitation (PPF). A large increase in EPSP1 amplitude and a decrease in rise time after tetanus is evident in Fig. 7A and Fig. 8A, respectively, which reflected LTP. LTP was typically accompanied by a reduction in N_0 (Fig. 7A). In addition, Fig. 7A (arrow) suggests appearance of EPSPs with a longer latency.

3.2.2. PCA application to physiological recordings

Fig. 7B–F illustrates PCA of the EPSPs shown in Fig. 7A. The notch in Fig. 7B (arrow) suggests existence of EPSPs with different latencies. Fig. 7C1 represents the first principal component loadings (f_1 , from Eq. (2)) reflecting essential features of the initial part of the average EPSP (Fig. 7B). The meaning of the second principal component loadings (Fig. 7C2) is more difficult to interpret. The C_1/C_2 scores are plotted in Fig. 7D. The shape of Fig. 7D (parallelogram similar the simulated bicomponent plots of Fig. 1Bb and Fig. 2Db) suggested a good component separation. Accord-

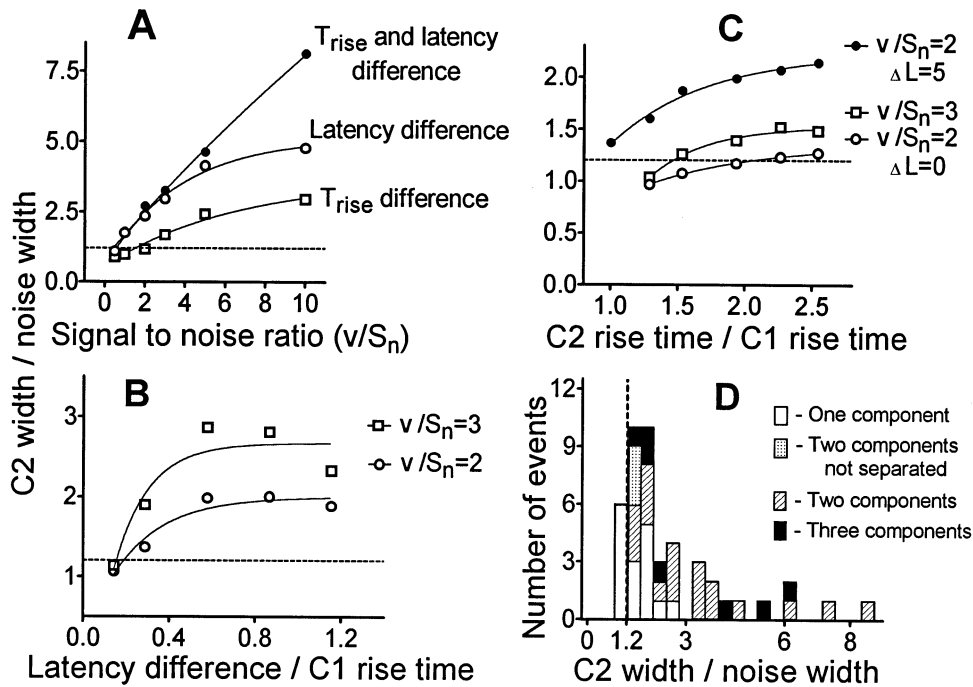


Fig. 6. Summary graphs of simulation and physiological experiments. (A–C) Relative width of the second component in C_1/C_2 graphs plotted against signal-to-noise ratios (A), relative latency differences (B) and relative rise times of the second component (C). The relative C_2 width is determined as the ratio of the width of the second component in C_1/C_2 graphs to that for the background noise. The latency (B) and T_{rise} (C) differences are expressed as their ratios to T_{rise} of the first component. Monoquantal components were simulated with $p = 0.5$ and various v/S_n . Different symbols in A represent simulations with $\Delta L/T_{rise} = 0.9$ and $T_{rise2}/T_{rise1} = 2.5$ (dots), $\Delta L/T_{rise} = 0.9$ (circles) and $T_{rise2}/T_{rise1} = 2.5$ (squares). T_{rise} or latencies were fixed in the experiments shown in B and C, respectively. (D) Distribution of the relative C_2 width in physiological experiments. The dashed lines in A–D indicates the criterion (1.2, see Section 3.1.1) for separation of plots with reliable and unreliable component separation.

ingly, its alignment represented no difficulties, and the aligned plot (Fig. 7E1) appeared to be similar to the simulated plots with quantal components (Fig. 1Db and Fig. 3Ab). Analogous plot for EPSP2 (Fig. 7E2) showed a smaller cloud around (0, 0) as compared to Fig. 7E1 reflecting PPF. To obtain C_1 (Fig. 7F1) we followed the procedure of Section 3.1.3 and averaged the waveforms corresponding to the dots along x -axes in Fig. 7E1. We performed analogous procedure to obtain C_2 (Fig. 7F2). C_1 and C_2 (Fig. 7F1 and 2) appeared to be alike in their waveforms but their latencies differed (2.3 and 5.4 ms, respectively). The responses from the cloud with positive x and y values in Fig. 7E1 could be interpreted as mixtures of the early and late components. Accordingly, their average (Fig. 7F3) was similar to the general average (Fig. 7A) and contained a notch (Fig. 7F3, arrow) corresponding to the expected transition between the components. The average (Fig. 7F4) corresponding to the cloud around 0 in Fig. 7E1 confirms that this cloud represented mostly failures and indicates the absence of additional independent components.

Existence of different components in another illustrated experiment (Fig. 8A) was suggested by the shape of the aligned plot (Fig. 8B) and confirmed by the average waveforms associated with the dots along the

x - and y -axes (Fig. 8C1 and C2, respectively). The latencies of the components were the same (2.2 ms) whereas their T_{rise} differed so that they were termed ‘slow’ and ‘fast’, respectively. Fig. 8D and E illustrate changes of their scores during the experiment.

3.2.3. Distribution of the recorded neurones according to PCA

Altogether the algorithm was applied to 45 EPSPs (300–2200 responses for each case). Fig. 6D shows that in six cases (the bar to the left of the dashed line) the width of C_2 in the C_1/C_2 plot was close to that of the noise plot. These cases (Fig. 9A) were similar to the plots of the simulated monoquantal EPSPs (Fig. 2Ab). Fig. 9Ac suggests that occasional large C_2 scores in Fig. 9Aa were due to spontaneous events. Comparison of the averages (Fig. 9Ab1 and 2) corresponding to different regions in Fig. 9Aa supports the existence of only one component.

The white bars to the right of the dashed line in Fig. 6D correspond to ten cases with both initial (Fig. 9Ba) and aligned (Fig. 9Bb) plots having structures typical for the simulations of variable waveforms (Fig. 2Bb and Fig. 3Bb, respectively). The averages of the responses associated with the dots along the x - and the y -axes and in the intermediate region (Fig. 9Bb1–3)

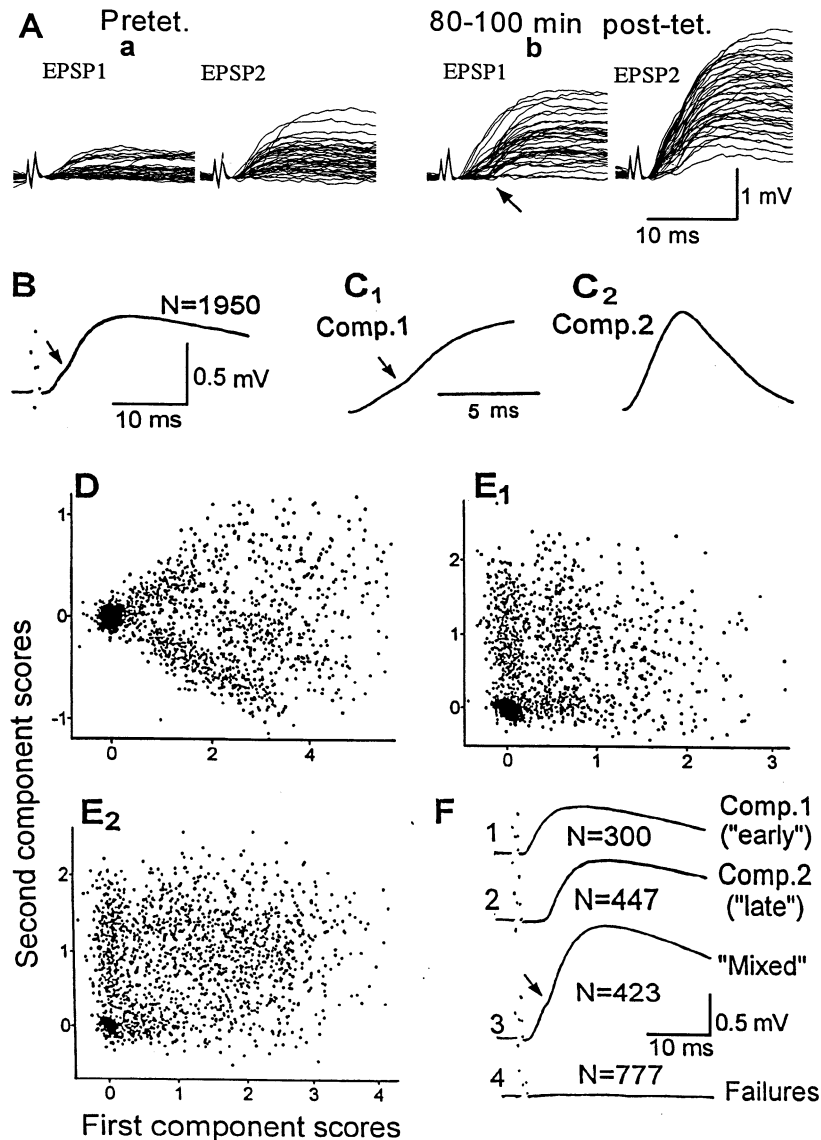


Fig. 7. Minimal EPSPs (A, B) and their component analysis (C–F). (A) Superpositions of consecutive single responses ($N = 50$) before (Pretet) and after (post-tet) tetanic stimulation. Responses to the first (EPSP1) and second (EPSP2) stimuli in the paired-pulse paradigm are shown. The resting membrane potential (MP) was -61 mV in the beginning and -64 mV at the end of the experiment; the input resistances (R) were 157 and 132 $M\Omega$, respectively. The small changes either in MP or R did not correlate with the amplitude changes. (B) Average waveform of all recorded EPSP1. The arrow marks a notch on the rising phase suggesting existence of two components. (C, D) First (C_1) and second (C_2) principal components' loadings and their scores (D) obtained after standard PCA. (E) scores of two initial components for EPSP1 (E1) and EPSP2 (E2) after the alignment procedure (Section 3.1.3). Note the square shape of the plots with gaps suggesting existence of separate (and quantal) components (compare with Fig. 3Ab). (F) Separation of EPSP1 into components using the procedure analogous to that illustrated in Fig. 3Ab. Similar to Fig. 1Db and 3Ab, the responses associated with dots along the x - (F1) and y -axes (F2) represent 'pure' short- and long-latency components, respectively; F3 represents their mixture (arrow marks a notch on the rising phase); F4 represents the average of the trials corresponding to the cloud around the coordinates (0, 0) in E1 (response failures).

suggest either strong waveform variations in one input or activation of a large number of presynaptic axons giving EPSPs with different T_{rise} . In six out of the ten cases, latency variations (for 1–3 ms) were also evident.

The dotted bars in Fig. 6D correspond to three cases with plots without clear borders which could not be reliably aligned (Fig. 9C). Nevertheless using the strategy elaborated in the simulation experiments (Fig. 5Cb) it was possible to distinguish these cases from the

waveform (or latency) variation (Fig. 9B) and to detect two components (Fig. 9Cb1 and 2) with different latencies (for 1, 3 and 3 ms). Differences in T_{rise} (for 5, 6 and 1.5 ms) were also evident in these 3 cases (compare Fig. 9Cb1 and 2). As mentioned above (Section 3.1.6), the scores of the individual components can not be used for reliable analysis in such cases.

The hatched and black bars in Fig. 6D represent the cases with two ($N = 19$) or three ($N = 7$) components differed in the latency (Fig. 7), T_{rise} (Fig. 8) or both.

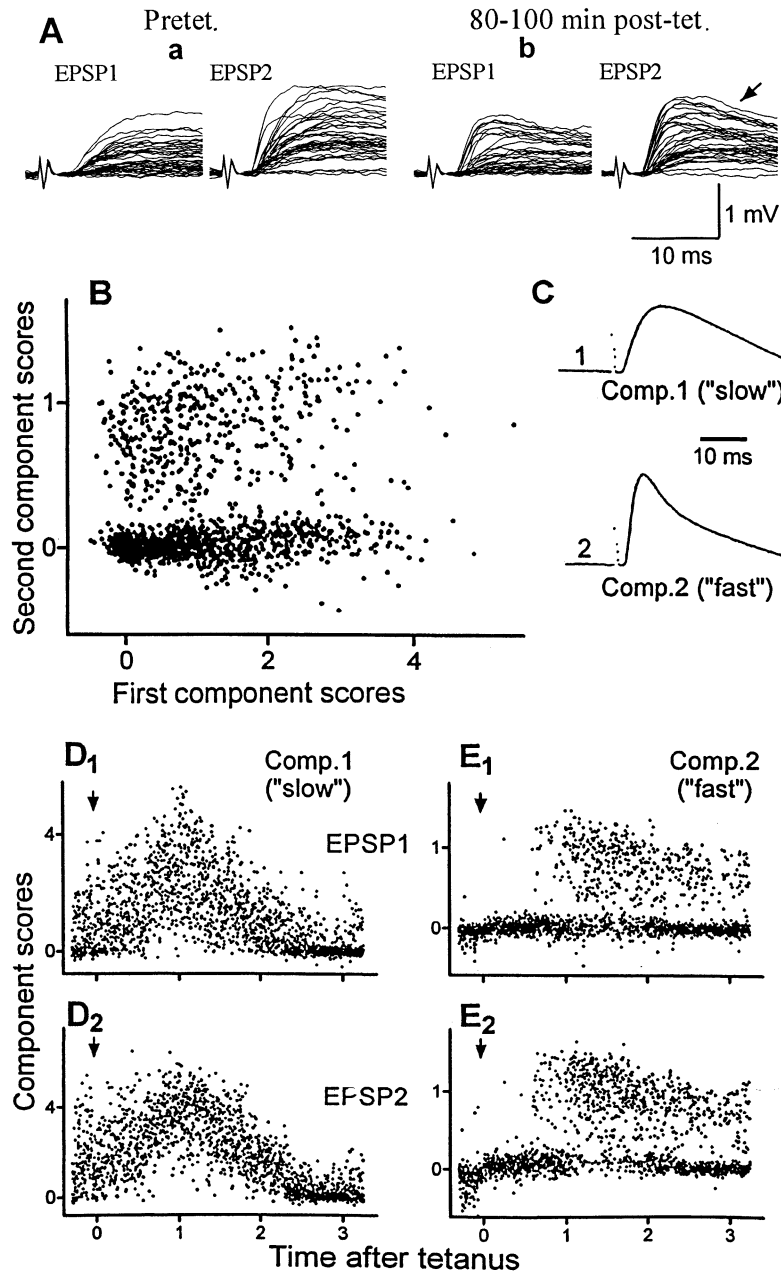


Fig. 8. Minimal EPSPs (A) and their component analysis (B–E) resulting in separation of two components with the same latency. (A) Superimposed EPSPs induced by paired pulses before and after tetanus as in Fig. 7A. MP was -62 mV in the beginning and -65 mV at the end of the experiment, R was 148 and 122 M Ω , respectively. (B) Plot of the scores of two initial components after the alignment procedure. (C) 'Pure' first (C_1) and second (C_2) components obtained by averaging the responses associated with dots along the x - and y -axes in B, respectively (see Fig. 1Db for more details). Note similar latencies but different kinetics of the 'slow' and 'fast' components. (D, E) scores of the first (D) and second (E) components plotted against time for EPSP1 (1) and EPSP2 (2). The arrow marks tetanization. Note similar potentiation time courses for the respective components of EPSP1 and EPSP2 but different changes for different components suggesting their association with different synapses.

Altogether the comparison of 40 component pairs gave eight cases with different (for 0.8–3.0 ms) latencies, but with T_{rise} similar within ≤ 1 ms (Fig. 7) which was close to the confidence interval for T_{rise} determination. T_{rise} varied from 4 to 9 ms (6.6 ± 1.9 , $N = 8$; mean \pm S.D., here and below) which gave the $\Delta L/T_{\text{rise}}$ ratios from 0.15 to 0.67 (0.36 ± 0.19 , compare with Fig. 6B).

In five pairs the components differed in T_{rise} (for 3 to 6 ms, 5.2 ± 1.3 ms) without any latency differences within the pixel size (0.2 ms). The latencies varied from 2.4 to 5.0 ms (3.5 ± 1.0 ms, $N = 5$). The other 27 pairs showed differences in both latencies (from 0.6 to 7.8 ms; 2.5 ± 1.8 ms) and T_{rise} (from 1.6 to 5.0 ms; 3.8 ± 1.7 ms).

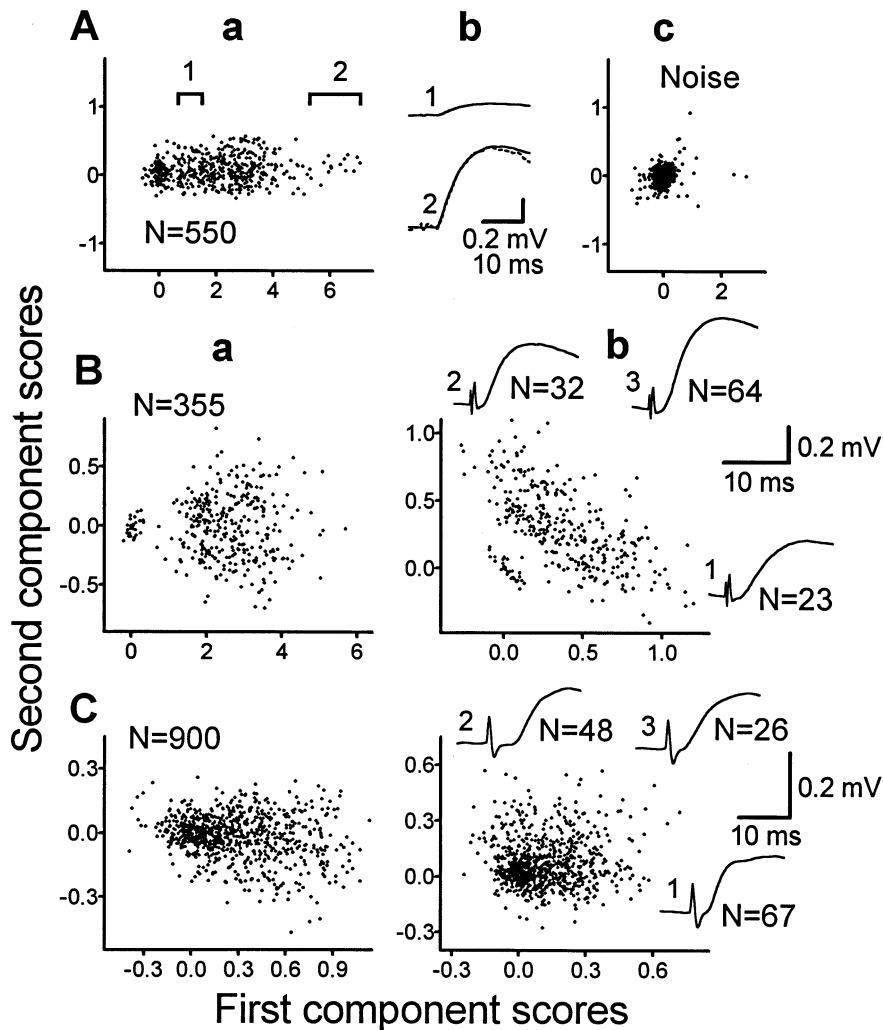


Fig. 9. Component analysis of three neurons representing a monocomponent EPSP (A), a variable waveform (B) and an EPSP consisting of two components with different latencies (C). The graphs represent C_1/C_2 plots before (Aa–Ca) and after their alignment (Bb, Cb) obtained from EPSP (Aa, B, C) and noise (Ac) measurements. (Aa) A band-like plot similar to the plots for simulated monocomponent EPSPs (compare with Fig. 1Db, 2A). 1 and 2 mark regions corresponding to small (presumably monoquantal) and large (multiquantal) responses, respectively. (Ab) Averages from the regions 1 and 2 in Aa. The dashed curve in Ab2 represents Ab1 scaled so that its peak amplitude matches that of Ab2 to show that the time courses are similar for the small (region 1 in Aa) and large (region 2 in Ab) EPSPs. (Ac) Component plot for the background noise obtained from the same sweeps as used for Aa but for prestimulus periods. Note that the width of the plot along the y-axis is similar to that in Aa suggesting the absence of a second component in Aa. (B) A 'fan'- (a) and a triangle- (b) like plots similar to the plots for the simulated waveform variations (compare with Fig. 2Bb and Fig. 3Bb). The meaning of 1–3 in Bb and Cb is the same as in Fig. 1Db. (C) A plot without clear borders not allowing complete separation of two waveforms. Nevertheless, the presence of two different waveforms rather than waveform variations was detected with comparison of averages from different parts of the plot (1–3 in Cb): the latency of the average from the intermediate part (Cb3) was as short as the latency of the average Cb1 rather than intermediate between the latencies of Cb1 and Cb2.

3.2.4. Behaviour of different components during LTP

The algorithm allowed us to study changes of the separate EPSP components resulting from different physiological and pharmacological challenges. Fig. 8D and E illustrate this possibility and show different post-tetanic changes of separate components. The 'slow' component was potentiated immediately after the tetanus (Fig. 8D), slightly increased during the first hour post-tetanus, was rather stable over about 1 h more and declined afterwards even below the pretetanic level. In contrast, the 'fast' component (Fig. 8E1) was

practically absent before tetanus: very rare large scores were visible only in responses to the second pulse (Fig. 8E2). Small responses appeared soon after tetanus (more clear in EPSP2, Fig. 8E2). Large responses appeared about 40 min later (Fig. 8E1). Note also only rare EPSP2 failures about 1.5 h post-tetanus (Fig. 8E2) and 'all-or-none'-like behaviour of both EPSP1 and EPSP2 so that mostly large and zero values appeared. The fast component (Fig. 8E) slowly declined afterwards, but the time-course of its decline was different from that of the slow component (Fig. 8D) and it

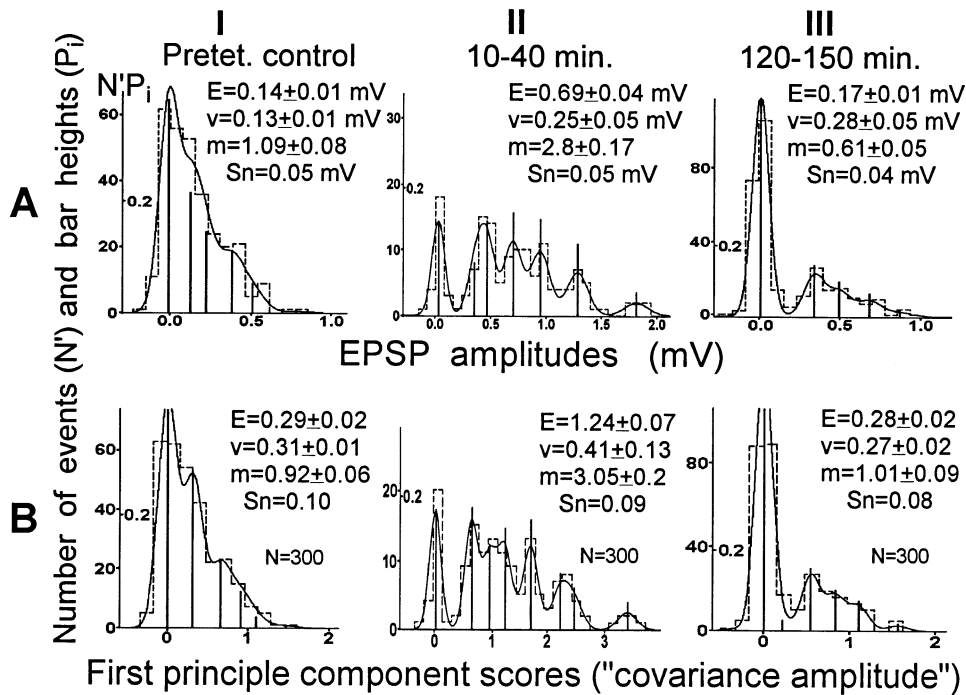


Fig. 10. Deconvolution analysis of the peak amplitudes (A) and of the first component scores (B). The latter were obtained with the standard PCA before the alignment procedure. The data were taken from the neurone shown in Fig. 7A. Experimental and predictive distributions are given by dashed and continuous lines, respectively. The deconvolved distributions are shown as bars (P_i refers to their probabilities). I–III correspond to different periods before (I) and after (II, III) tetanus. The insets give the mean amplitude (E), estimated quantal size (v), mean quantal content (m), noise S.D. (S_n) and sample size (N , see B). Note more regular distances between the bars in B (I and III) as compared to A but similar m values (except region III) and general similarity of the amplitude changes.

persisted until the end of the recording. The delayed (for 15–60 min) but persistent potentiation of one component (Fig. 8E and Fig. 11D) with the immediate but decremting (after about 1.5 h) potentiation of the other one was observed in both illustrated neurones (Figs. 8 and 11) and in several other cases which will be analyzed in details elsewhere.

3.3. Deconvolution analysis of the component scores

Dashed lines and bars in Fig. 10A show peak EPSP amplitudes and deconvolution solutions, respectively. Although the distances between the bars were not always uniform, the formal analysis showed about two-fold increase in v after tetanus (Fig. 10AII) with a larger increase in m . The predominant increase in m agrees with our previous results obtained with both sharp electrode (Voronin, 1993) and whole cell (Astrelin et al., 1997; Voronin et al., 1997) recordings (see also Stevens, 1993; Voronin, 1993; Larkman and Jack, 1995 for similar results of other groups). Fig. 10B shows the analysis of initial C_1 scores obtained before their alignment. The general result was similar to that in Fig. 10A although the distances between the bars were more uniform and the relative post-tetanic increase in v was smaller (Fig. 10BII) and non-existent for the later LTP period (Fig. 10BIII).

Fig. 11 illustrates PPF (Fig. 11A, B) and quantal analysis (Fig. 11C and D) of the separate components of the same EPSP. We stress several points which were not possible to see from the analysis of the compound measurements (Fig. 10). (1) Transient potentiation of the early component (Fig. 11A and C). (2) Very large persistent LTP of the late component, especially for EPSP1 which was practically absent before tetanus (Fig. 11B, x -values, 11D1) so that it represented a ‘virtually silent’ synapse before LTP induction. However, the scores of the EPSP2 components were significantly different from 0 before tetanus (Fig. 11BI, y -values, Fig. 11D2,I) so that the synapse was ‘presynaptically’ (Torii et al., 1997) rather than ‘postsynaptically silent’ (Durand et al., 1996). (3) No significant v increases for either first (Fig. 11CII) or second (Fig. 11D2,II) component during the early LTP period. (4) About two-fold increase in the estimated v for the late EPSP2 component lately post-tetanus (Fig. 11D2,III) as compared to the pretetanic period (Fig. 11D2,I, see also Fig. 11D1,III).

4. Discussion

We applied PCA to minimal EPSPs. One peculiarity of this application in comparison with the previous

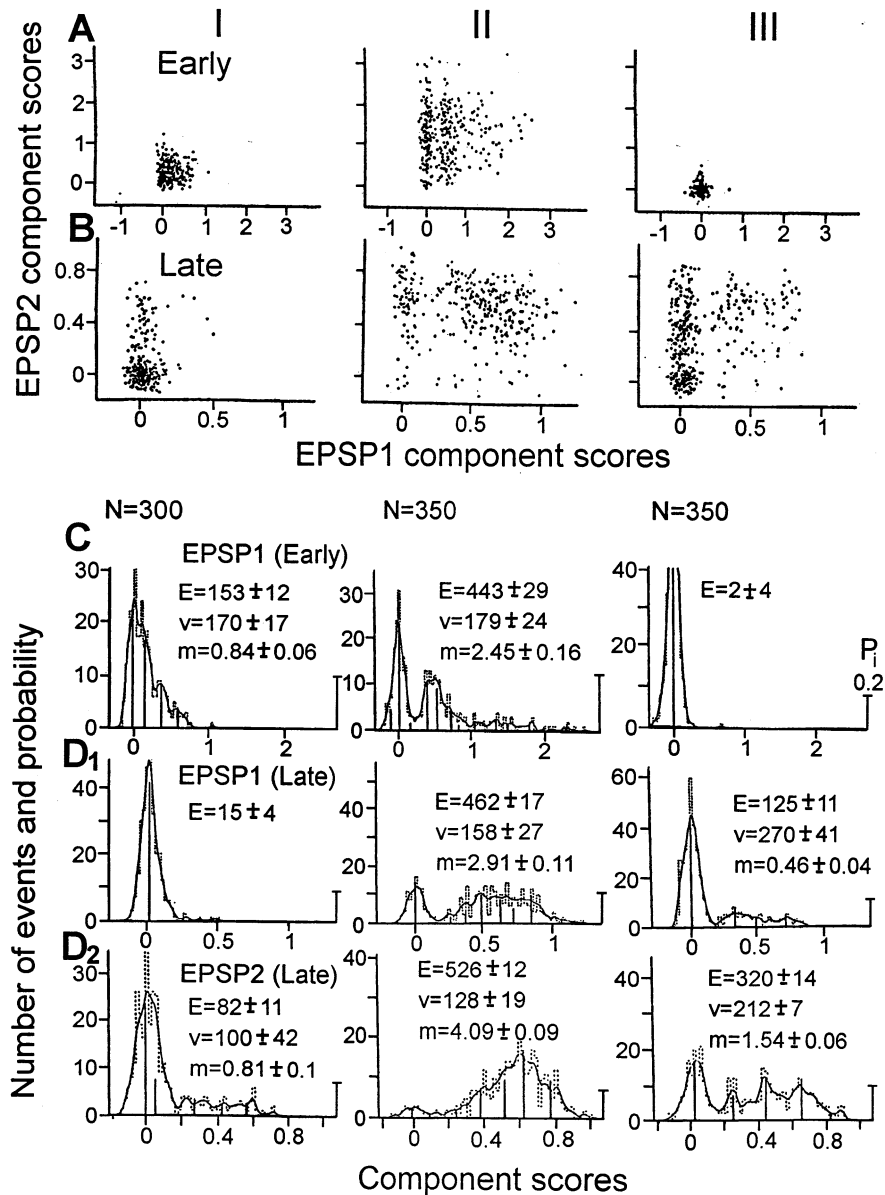


Fig. 11. Plots of component scores for two EPSPs in the paired pulse paradigm (A, B) and deconvolution analysis of separate components (C, D). Similar to Fig. 10, the data were taken from the experiment illustrated in Fig. 7A but the separate scores of the early and late components (Fig. 7F) were used. Comparison of the pretetanic (I) and post-tetanic (II, III) regions in A and B demonstrates very large (AII) but transient (AIII) potentiation of the early component and persistent potentiation of the late component (BII, III). The deconvolution analysis (C, D) is shown for the EPSP1 of the early component and for both EPSP1 (D1) and EPSP2 (D2) of the late component. The scales for bars ($P_i = 0.2$, see CIII) are given to the left of each graph. See Fig. 10 for other notations. Quantal parameters for CIII and D1,I are not given because of very small number of positive scores ('virtually silent' synapses, see below). Note that for the early component (C1,II) the estimated v did not change significantly after tetanus, whereas for the late component (D2) the apparent v increased about twofold during the late LTP period (D2,III) as compared to the pretetanic control (D2,I). Note also that the late component was almost non-existent before tetanus if one considers EPSP1 (B1, D1) i.e. it represented a 'virtually silent' synapse. However, occasional large EPSP2 (B1, D2,I) suggest that active postsynaptic receptors were present and the synapse was 'presynaptically silent'.

electrophysiological studies (Glaser and Ruchkin, 1976; Barth and Di, 1992; Chapman and McCrary, 1995) is that we used single (non-averaged) responses as the input data. Therefore the results can be used for further analysis of single trials. The standard PCA (Fig. 1B) gives C_1 scores which can be used instead of conventional amplitude or slope measurements. Such 'covari-

ance amplitudes' (Fig. 10B) utilize more information about the waveform and are more reliable as compared to the conventional measures (Chapman and McCrary, 1995).

As noted by many authors who recorded electrical evoked potentials (e.g. Collet, 1989), the physiological meaning of the PCA components might be uncertain.

To facilitate the interpretation we elaborated procedures for extraction of distinct waveforms. We showed that hippocampal minimal EPSPs can be often separated into two components with different latencies and/or time courses. The simplest interpretation of this result is activation of more than one presynaptic fibre or release site (see Section 1, Introduction). Indeed, even a single axon branch can contact two to four different dendrites of a target CA1 neurone (Harris and Kater, 1994) so that the related synapses can be spatially remote and produce EPSPs with different latencies and kinetics. In addition to the Schaffer collaterals and local circuit connections (Thomson and Deuchars, 1995) polysynaptic pathways can be activated. Their activation demands further analysis but our preliminary evaluations showed approximately similar latency variations for early and late components. We believe that significant polysynaptic activation was unlikely under our conditions (minimal stimulation, TTX, cut between CA3 and CA1).

The interpretation of the EPSP components based on activation of different synaptic sites is supported by our simulation experiments with known component number and characteristics. The plots of the component scores appeared to be strikingly similar in the simulation and physiological experiments. Several additional observations are compatible with physiological meaningfulness of the EPSP components. (1) When different components were suspected from considerations of single (Fig. 7A) or average (Fig. 7B) responses, PCA produced expected components. (2) Comparison of EPSP1 and EPSP2 gave expected results: the same respective components, characteristic PPF, parallel post-tetanic changes, smaller post-tetanic increases for EPSP2 as compared to EPSP1 scores. The later observation agrees with post-tetanic decreases in PPF under our conditions (Sokolov et al., 1997; see also Kuhnt and Voronin, 1994; Kleschevnikov et al., 1998). (3) Dissimilar changes of different components with time confirm that they represented independent identities. (4) PCA of the background noise produced about zero scores with occasional large values which typically corresponded to spontaneous events similar to EPSPs by their waveforms. (5) Responses with about zero scores usually represented failures.

The existence and heterogeneous behaviour of different components have several implications. As an example we shall briefly discuss their relation to LTP phases (Bliss and Collingridge, 1993; Reymann, 1993). Our recording period corresponded to two presumed phases: LTP1 (termed also STP which covers initial 15–60 min according to different works) and LTP2 (which develops slower and lasts up to 3–4 h). There is no general agreement on LTP1 and LTP2 mechanisms. For example, LTP1 was explained by primarily pre- (Bliss and Collingridge, 1993; Voronin, 1993; Kullmann et al.,

1996) or postsynaptic (Malenka and Nicoll, 1993; Edwards, 1995; Xiao et al., 1996) modifications. The present data suggest a new view indicating that different synaptic sites (or even inputs) may be responsible for different phases. The delayed (15–60 min) potentiation of one of the components suggests that LTP2 may be due to morphological changes. Appearance of synapses with completely separated transmission zones (Geinisman et al., 1993) represents a plausible possibility (see Edwards, 1995; Voronin et al., 1995). These synapses may synchronously release two or several quanta and produce large EPSPs with ‘all-or-none’ behaviour (Volgushev et al., 1995). Both the characteristics of the components with delayed LTP (Fig. 8E, 11BIII, compare with figure 2b and figure 6b in Volgushev et al., 1995 respectively) and apparent v doubling (Fig. 11D2) are consistent with this scenario (see Voronin et al., 1995; Kleschevnikov et al., 1997 for additional discussions).

Summarizing, we demonstrated that PCA is applicable to minimal EPSPs. We described procedures which separate physiologically meaningful EPSP components presumably arising from activation of different fibres or release sites. Under realistic signal-to-noise ratios ($> 2-3$) the algorithm can resolve components with about 0.8–1 ms latency or about 3 ms T_{rise} differences. In practice the sensitivity is often even higher (0.6 and 1.6 ms, respectively) because differences in both latency and T_{rise} are common. From the methodological point of view, the PCA application can be considered as a way to substitute recordings of single fibre EPSPs for a less laborious and more stable recordings of minimal EPSP. In addition, the component analysis can be used for more precise analysis of unitary PSPs separating activation of different transmission zones.

Acknowledgements

We thank Drs. A.M. Kleschevnikov, M.A. Kulikov and A.V. Rossokhin for participation in parts of this work, C. Patton for improving the English and the anonymous referees for valuable suggestions. This work was supported by a grant from Volkswagen Stiftung to K.G.R. and L.L.V. and a grant from the Russian Foundation for Basic Researches (RFBR) to L.L.V.

References

- Alger BE, Pitler TA, Wagner JJ, Martin LA, Morishita W, Kirov SA, Lenz RA. Retrograde signalling in depolarization-induced suppression of inhibition in rat hippocampal CA1 cells. *J Physiol London* 1996;496:197–209.
- Astrelin AV, Sokolov MV, Behnisch T, Reymann KG, Voronin LL. Noise deconvolution based on the L1-metric and decomposition of discrete distributions of postsynaptic responses. *J Neurosci Methods* 1997;73:17–27.

- Barth DS, Di S. Topographical analysis of epileptiform potentials in rat somatosensory cortex: the interictal to ictal transition. *Brain Res* 1992;591:33–43.
- Bliss TVP, Collingridge GL. A synaptic model for memory: long-term potentiation in the hippocampus. *Nature* 1993;361:31–9.
- Chapman RM, McCrary JW. EP component identification and measurements by principal components analysis [Review]. *Brain Cognit* 1995;27:288–310.
- Chapman RM, McCrary JW, Tuttle JR. Principal components analysis of variability in retinal ganglion cell responses. *Biol Cybern* 1981;42:45–50.
- Churchland PS, Sejnowski TJ. *The Computational Brain*. Cambridge, MA: MIT Press, 1992.
- Collet W. Doubts on the adequacy of the principal component varimax analysis for the identification of event-related brain potential components: a commentary on Glaser and Ruchkin, and Donchin and Heffley. *Biol Psychol* 1989;28:163–72.
- Durand GM, Kovalchuk Y, Konnerth A. Long-term potentiation and functional synaptic induction in developing hippocampus. *Nature* 1996;381:71–5.
- Edwards FA. LTP—a structural model to explain the inconsistencies. *Trends Neurosci* 1995;18:250–5.
- Edwards FA, Konnerth A, Sakmann B. Quantal analysis of inhibitory synaptic transmission in the dentate gyrus of rat hippocampal slices: a patch clamp study. *J. Physiol* 1990;430:213–49.
- Friston KJ. Computational approaches to quantifying human neuroanatomical variability. In: Toga AW, Mazziotta JC, editors. *Brain Mapping*. San Diego: Academic Press, 1996;363–385.
- Geinisman Y, de Toledo-Morell L, Morell F, Heller RE, Rossi M, Parshall RF. Structural synaptic correlate of long-term potentiation: formation of axospinous synapses with multiple, completely partitioned transmission zones. *Hippocampus* 1993;3:435–46.
- Glaser EM, Ruchkin DS. *Principles of Neurobiological Signal Analysis*. New York: Academic Press, 1976.
- Harmon HH. *Modern Factor Analysis*, 3rd edn. Chicago: University of Chicago Press, 1979.
- Harris KM, Kater SB. Dendritic spines—cellular specializations imparting both stability and flexibility to synaptic function. *Ann Rev Neurosci* 1994;17:341–371, 498–520.
- Hotellin H. Analysis of a complex of statistical variables into principal components. *J Ed Psychol* 1933;24:417–41.
- Jackson JE. *A User's Guide to Principal Components*. New York: John Wiley, 1991.
- Kleschevnikov AM, Sokolov MV, Kuhnt U, Dawe GS, Stephenson JD, Voronin LL. Changes in paired-pulse facilitation correlated with induction of long-term potentiation in area CA1 of rat hippocampal slices. *Neuroscience* 1997;76:829–43.
- Korn H, Faber DS. Quantal analysis and synaptic efficacy in the CNS. *Trends Neurosci* 1991;14:439–45.
- Kuhnt U, Voronin LL. Interaction between paired-pulse facilitation and long-term potentiation in area CA1 of guinea pig hippocampal slices: application of quantal analysis. *Neuroscience* 1994;62:391–7.
- Kullmann DM. Quantal variability of excitatory transmission in the hippocampus: implications for the opening probability of fast glutamate-gated channels. *Proc R Soc London* 1993;B253:107–16.
- Kullmann DM, Erdemli G, Asztely F. LTP of AMPA and NMDA receptor-mediated signals: evidence for presynaptic expression and extrasynaptic glutamate spill-over. *Neuron* 1996;17:461–74.
- Larkman AU, Jack JJB. Synaptic plasticity: hippocampal LTP. *Curr Opin Neurobiol* 1995;5:324–34.
- Malenka RC, Nicoll RA. NMDA-receptor-dependent synaptic plasticity: multiple forms and mechanisms. *Trends Neurosci* 1993;16:521–7.
- Martin AR. Quantal nature of synaptic transmission. *Physiol Rev* 1966;46:51–66.
- Raastad M. Extracellular activation of unitary excitatory synapses between hippocampal CA3 and CA1 pyramidal cells. *Eur J Neurosci* 1995;7:1882–8.
- Redman S. Quantal analysis of synaptic potentials in neurons of the central nervous system. *Physiol Rev* 1990;70:165–98.
- Reymann KG. Mechanisms underlying synaptic long-term potentiation in the hippocampus: focus on postsynaptic glutamate receptors and protein kinases. *Funct Neurol* 1993;8(S5):7–32.
- Sokolov MV, Rossokhin AV, Behnisch T, Reymann KG, Voronin LL. Interaction between paired-pulse facilitation and long-term potentiation of minimal EPSPs in rat hippocampal slices: a patch clamp study. *Neuroscience* 1998 (in press).
- Stevens CF. Quantal release of neurotransmitter and long-term potentiation. *Cell/Neuron* 1993;70(Suppl):55–63.
- Stern P, Edwards FA, Sakmann B. Fast and slow components of unitary EPSCs on cells elicited by focal stimulation in slices of cortex. *J Physiol* 1992;449:247–78.
- Stricker C, Field AC, Redman S. Changes in quantal parameters of EPSCs in rat CA1 neurones in vitro after the induction of long-term potentiation. *J Physiol* 1996;490:443–54.
- Thomson AM, Deuchars J. Diverse pre- and post-synaptic properties of fast excitatory synapses. In: Thomson AM, Deuchars J, editors. *Excitatory Amino Acids and Synaptic Transmission*. London: Academic Press, 1995:146–172.
- Torii N, Tsumoto T, Uno L, Astrelin AV, Voronin LL. Quantal analysis suggests presynaptic involvement in expression of neocortical short- and long-term depression. *Neuroscience* 1997;79:317–21.
- Volgushev M, Voronin LL, Chistiakova M, Artola A, Singer W. All-or-none excitatory postsynaptic potentials in the rat visual cortex. *Eur J Neurosci* 1995;7:1751–60.
- Voronin LL. On the quantal analysis of hippocampal long-term potentiation and related phenomena of synaptic plasticity. *Neuroscience* 1993;56:275–304.
- Voronin LL, Kuhnt U, Hess G, Gusev A, Roschin V. Quantal parameters of 'minimal' excitatory postsynaptic potentials in guinea pig hippocampal slices: binomial approach. *Exp Brain Res* 1992;89:248–64.
- Voronin LL, Ivanov NV, Kuhnt U. Estimate of the variance of the quantal size in excitatory synapses of area CA1 of hippocampal slices. *Neurophysiology* 1993;1:10–7.
- Voronin L, Byzov A, Kleschevnikov A, Kozhemyakin M, Kuhnt U, Volgushev M. Neurophysiological analysis of long-term potentiation in mammalian brain. *Behav Brain Res* 1995;66:45–52.
- Voronin LL, Volgushev M, Chistiakova M, Kuhnt U, Singer W. Involvement of silent synapses in the induction of LTP and LTD in hippocampal and neocortical neurones. *Neuroscience* 1996;74:323–30.
- Voronin LL, Kleschevnikov AM, Sokolov MV, Kasianov AM, Astrelin AV, Rossokhin AV. Synaptic mechanisms of the early and late phases of hippocampal long-term potentiation (LTP). XXXIII International Congress of Physiological Science, St. Petersburg, Abstract L075.04. 1997.
- Wahl LM, Stratford KJ, Larkman AU, Jack JJB. The variance of the successive peaks in synaptic amplitude histograms: effect of intersite difference in quantal size. *Proc R Soc London* 1995;B262:77–85.
- Walmsley B. Quantal analysis of synaptic transmission. In: Wallis DI, editors. *Electrophysiology—A Practical Approach*. Oxford: IRL Press, 1993:110–141.
- Walmsley B. Interpretation of 'quantal' peaks in distributions of evoked synaptic transmission at central synapses. *Proc R Soc London* 1995;B261:245–50.
- Xiao MY, Niu YP, Wigstrom H. Activity-dependent decay of early LTP revealed by dual EPSP recording in hippocampal slices from young rats. *Eur J Neurosci* 1996;8:1916–23.